Received: 12 October 2023 | Accepted: 27 November 2023

DOI: 10.1002/jemt.24473

RESEARCH ARTICLE

MICROSCOPY RESEARCH & TECHNIQUE WILEY

A novel image processing procedure for the quantitative evaluation of dental enamel prism arrangement

Máté Hegedűs[1] | Viktória K. Kis[2,3] | Noémi Rózsa[4] | Zsolt Kovács[1]

[1]Department of Materials Physics, Eötvös Loránd University, Budapest, Hungary

[2]HUN-REN Centre for Energy Research, Budapest, Hungary

[3]Department of Mineralogy, Eötvös Loránd University, Budapest, Hungary

[4]Faculty of Dentistry, Department of Pedodontics and Orthodontics, Semmelweis University, Budapest, Hungary

Correspondence
Máté Hegedűs, Department of Materials Physics, Eötvös Loránd University, H-1117 Budapest, Pázmány Péter stny 1/a, Hungary.
Email: hegmat@student.elte.hu

Funding information
National Research, Development and Innovation Fund Office, Hungary

Review Editor: Paul Verkade

Abstract

Enamel prism is the main microstructural unit of mammalian enamel which composed of hundreds of bioapatite nanocrystals. Prism structure plays a key role in the excellent mechanical performance of dental enamel during millions of chewing cycles without significant remodeling. Thus, quantitative understanding of prism architecture is of utmost importance for biomechanical materials design. To characterize enamel prism orientation quantitatively, a novel image processing method has been developed. Our method is based on scanning electron microscopy images of etched enamel surface and consists of an ellipse fitting procedure, which provides a numerical approximation of prism shape and orientation in the studied cross section. The obtained analytical data allow to construct color coded orientation maps, which provide quick and useful insight into the microstructure of enamel. Besides striking visualization, orientation maps allow to extract and plot the rich information on the azimuthal and inclination angles of the prisms as function of location. Numerical data on prism arrangement can be analyzed using statistical tools over large areas, which paves the way towards quantifying comparative investigation of prism arrangement either in dentistry research or evolution biology. The application of the method is demonstrated for a distal–mesial cross-section of sound human tooth enamel.

Highlights

- Scanning electron microscopy images of etched enamel surface are analyzed using ellipse fitting.
- Geometrical parameters of the fitted ellipses provide numerical data of thousands of prisms.
- Prism arrangement is visualized on color coded orientation maps and analyzed using statistical tools.

KEYWORDS
enamel microstructure, Hunter-Schreger bands, image processing, prism orientation

1 | INTRODUCTION

Tooth enamel is the hardest and most mineralized tissue of vertebrates. The complex microstructure of enamel contains needle-shaped hydroxyapatite (HAP) crystals of about 68 × 26 nm size in cross section (Daculsi & Kerebel, 1978) with length up to 10 μm (Daculsi et al., 1984). Nanocrystals are arranged on several structural levels to form the most characteristic unit of mammalian dental enamel, the enamel prism (Cui & Ge, 2007; Nanci, 2017). Prisms are the main microscale building blocks of enamel and typically have diameter of few micrometers in cross-section (Wilmers & Bargmann, 2020). Prisms extend from the dentin-enamel junction (DEJ) up to the enamel external surface and their pathway has a wavy character (Besnard, Marie, Bucek, et al., 2022; Radlanski et al., 2001), as controlled by the activity of enamel producing cell ameloblast, during amelogenesis (Lester & von Koenigswald, 1989). As a consequence of the wavy pathway, on a longitudinally sectioned tooth surface, special patterns can be observed. In human enamel, prisms with identical orientations are arranged into few tens of micrometer thick groups and appear as periodic dark and light bands under light microscope (Hunter-Schreger band, HSB) due to the orientation dependent refractive index of the prism forming nanocrystals (Osborn, 1965). Prism patterns are believed to develop as an adaptive response to biomechanical stresses related to nutrition habits (Rensberger & W. von., 1980). The first proof of functional differentiation of prism patterns between incisor and molar has been observed in case of a late Cretaceous mammal Mesodma (Sahni, 1987a). Clear prismatic microstructure with developed HSBs was reported from the Middle Eocene whales (Ishiyama, 1984).

Prism structure plays a key role in making up mechanical behavior of enamel, which can survive millions of chewing cycles with forces between 28 and 1200 N (Ferrario et al., 2004) despite the existing cracks (He et al., 2013). The wavy prism arrangement and the related nanocrystal misorientation contribute to increase crack resistance, as proven by cyclic loading experiments performed on human molar (Bajaj & Arola, 2009), and molecular dynamics simulations (Beniash et al., 2019), respectively. Synchrotron coupled in-situ indentation measurements accompanied by finite element model simulations indicated the influence of underlying structure on the mechanical response (Salvati et al., 2019).

Average nanocrystal orientation changes gradually over enamel cross section showing a spectacular pattern highlighting prism boundaries (Beniash et al., 2019). The effect of crystal structure anisotropy of HAP on mechanical properties was investigated using multiscale simulations (An et al., 2012). In fact, fracture toughness, as function of nanocrystal orientation was recently measured as well using FIB-milled enamel micropillars of different orientation (Chu et al., 2021).

As teeth serve as tools for feeding, and sometimes also as weapons, dietary habits are reflected in enamel microstructure. Soft food feeder animals are likely to have relatively simple radial structure and less decussation than hard food feeders (Lucas et al., 2008) and they also possess thinner enamel (Smith et al., 2012). Evolutionary adaptation allows to conclude dietary habits based on enamel macro- (Evans et al., 2006) and microstructure. Moreover, enamel prisms preserve their growth circumstances by micro features related to circadian rhythm, which are not overwritten by remodeling (Tafforeau et al., 2012).

The microstructure of human enamel, that is, HSB patterns and alternating prism orientation have been widely investigated over a century by various microscopy techniques, however, the quantitative investigations are scarce. HSB packing density based on light microscopy measurements was found to be greater at those regions where occlusal load was higher due to mastication (Lynch et al., 2010). Recently, based on scanning electron microscopy (SEM) images a similar study concluded that that mandibular molars exhibit weaker decussation than maxillary (Yang et al., 2022). Quantitative evaluation of optical micrographs taken with circularly polarized light has proven to be useful for HSB analysis (Hogg & Richardson, 2019). This technique revealed differences of enamel complexity in case of different monkey species, which was attributed to different masticatory loads (Hogg & Elokda, 2021). Mouse enamel was investigated using SEM micrographs by measuring precisely the angle and number of prisms and the complexity of their arrangement was discussed (Smith et al., 2019).

In this paper we present a novel method based on SEM micrographs, which facilitates the quantitative investigation of prism microstructure. It is demonstrated that by combining a simple and easily available instrumentation—scanning electron microscope—with image processing procedure, the spatial variation of prism orientation in dental enamel can be mapped. The orientation maps are constructed using analytical shape and area parameters, which allows to describe quantitatively the spatial variation of prism orientation and provides access to a statistical analysis of HSBs over large areas as well.

2 | METHODOLOGY

2.1 | Materials and sample preparation

Human primary teeth were provided by donation. The research procedure was approved by the Ethics Committee of the Semmelweis University, Budapest (approval no. 84/2020). A sound molar was embedded in diphase dentacryl resin (SpofaDental Inc., Czech Republic). Cutting was performed with an Accutom-100 cutting machine (Struers, Denmark) equipped with a diamond sawing disc. The molar was divided into two halves, with the cut surfaces lying perpendicular to the distal-mesial division line. The cut surfaces of each halves were then grinded using a motorized LaboPol-20 polishing and grinding machine (Struers, Denmark) with silicon carbide grinding discs (P1200, P2400, P4000) by 250 rpm. Polishing cloths were used for the final step with aluminum oxide suspension with decreasing grain size (1 μm, 0.3 μm). Between each step, the specimen was gently cleansed under running water.

2.2 | Scanning electron microscopy

Imaging of cross-sectional enamel surface was performed by using an FEI Quanta 3D FEG dual beam electron microscope (Schottky-type electron gun with a 20 kV acceleration voltage and 20 pA current). The surface of the enamel was etched using hydrochloric acid (10%) three times for a total of 2 min in order to make prism edges visible with clean edges in the scanning electron microscope (SEM). Selection of etching time was chosen based on Arnold et al. (2015). Water vapor was released into the sample chamber to reduce the charging effect on the specimen surface. LVSED (low-vacuum secondary electron detector) detector was used for the detection of secondary electrons (SEs).

3 | IMAGE PROCESSING

3.1 | Prism orientation map construction method

Proper etching procedure of enamel surface develops prism boundaries, which can be imaged by SEs in the SEM. Fine surface morphology is enhanced by local intensity maxima due to the higher SE yield on the edges and apexes. Thus, enamel prisms appear separated by high contrast lines, which allows the identification of each prism in an SE image by image processing. For a step by step demonstration of the image processing, a relatively small, 100 × 100 μm region of a high resolution SEM image was selected (Figure 1a). The image processing was carried out using ImageJ software (v1.53v version) as detailed in the following points.

- Brightness and contrast were adjusted on the image to improve the visibility of the high intensity edges and decrease all the other contrast. For larger images, brightness and contrast were adjusted for smaller areas independently to compensate for the slightly uneven spatial electron yield at different parts of the image.
- Thresholding of intensity values was performed in a way to find the intensity maxima of practically all enamel prism (see the blue dots in Figure 1a). Maxima are ignored if they do not stand out from the surroundings by more than the selected threshold value. These intensity maxima are the less solved parts of the surface, which are located inside the prisms, as seen in Figure 1a.
- An area was assigned to each intensity maxima by a segmentation procedure. The boundary between these areas can be considered as virtual prism boundaries (Figure 1b). These segmented areas have complex shapes with irregular boundaries.

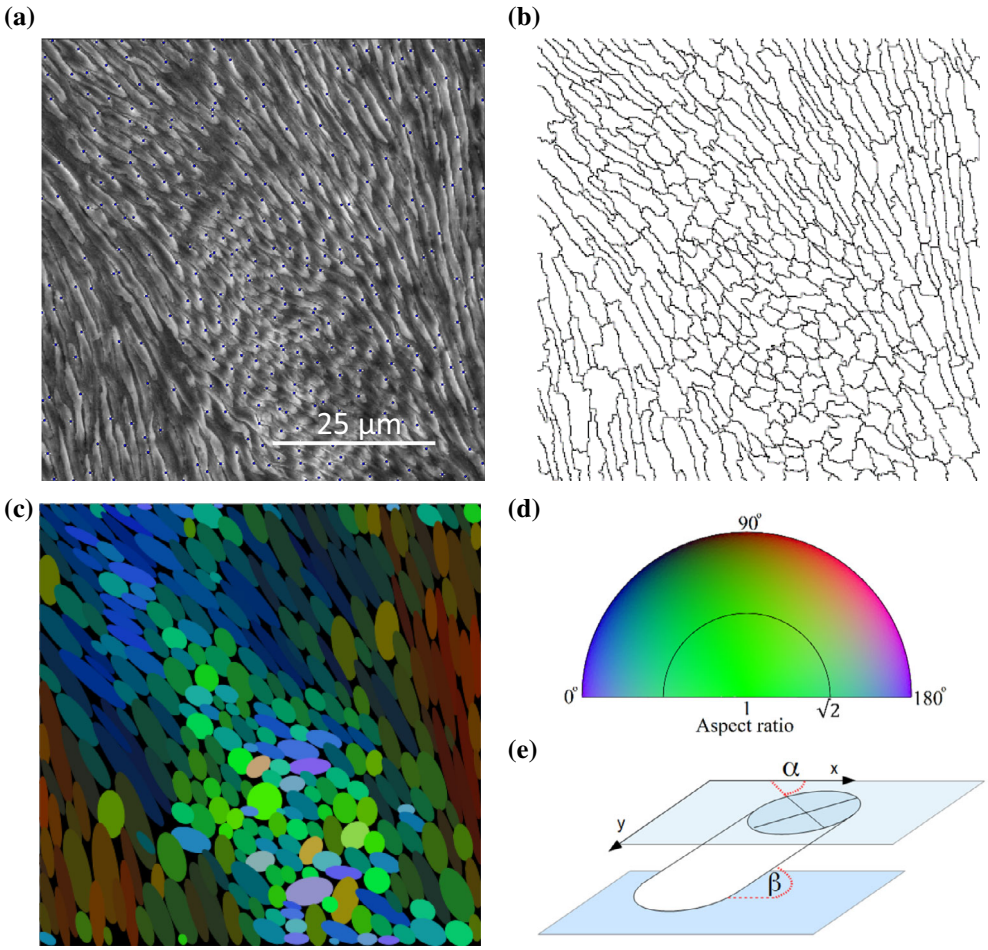

FIGURE 1 Selected part of a secondary-electron SEM image of a bucco-lingual section of a human sound molar enamel (the whole image will be shown in Figure 4a) Local intensity maxima due to the higher secondary-electron yield are indicated by blue dots (a). Virtual prism boundaries are defined by segmentation procedure (b). Orientation map color based on the aspect ratio and azimuthal angle of fit ellipses (c). An explanatory diagram shows the color code of ellipse fitting parameters (the aspect ratio and the azimuthal angle) (d). A schematic illustration of a single cylindrical prism with α azimuthal and β tilt angles and its elliptical cross section with the fit ellipse (e).

- In order to get analytical shape and area parameters for the prisms, the following approximation was made. Each prism is considered as a simple cylinder with infinite length. The cross-section of this cylinder with the images surface is an ellipse and the ratio of its major and minor axis (aspect ratio, AR) varies as a function of the angle between the cylinder long axis and the surface normal (tilt angle, **β**). Based on this approximation, ellipses were fit to each segmented area as seen in Figure 1c. The ellipses close to AR ≈ 1 represent prisms with elongation direction nearly parallel to the incident electron beam, while ellipses with larger aspect ratio indicates the tilt of prism elongation direction away from the direction of the incident beam. The ellipse fitting process provides automatic and quick access to the numerical parameters of each ellipse like (*x*,*y*) centre coordinates, length of the major/minor axis, the aspect ratio, the area and the azimuthal angle (**α**) of the major axis.
- For detailed characterization and visualization of prism arrangement, an orientation map can be constructed by plotting each ellipse with a color code. The RGB color code is based on the azimuthal angle, which varies in the range of $\alpha = 0–180^\circ$ (red and blue components) and the aspect ratio (green), which is related to the vertical prism inclination (Figure 1d) by $\beta = \arcsin(1/AR)$. Color code is defined as

$$R = \cos(\beta)\cdot\frac{1}{2}(\sin(2\cdot\alpha)+1)\cdot 256 \quad (1)$$

$$G = \sin(\beta)\cdot 256 \quad (2)$$

$$B = \cos(\beta)\cdot\frac{1}{2}(\cos(2\cdot\alpha)+1)\cdot 256 \quad (3)$$

- A schematic illustration shows the relationship between the color code and ellipse parameters (Figure 1e). Keeping in mind the simplification related to the prism shape in the present procedure, full 3D information on the prism arrangement can be obtained.

Based on Equations (1)–(3), the ellipse parameters can also be calculated back from the RGB values in a selected area of the orientation map and plotted as function of position. Hence, area averaged information can be easily deduced from the colored maps. In this way, an orientation map (Figure 1c) provides rich information on the spatial arrangement of thousands of enamel prisms.

3.2 | Analysis of the method and limitations

The presented method for enamel prism arrangement analysis has some limitation factors. The high efficiency separation of intensity maxima requires SE images of appropriate resolution. Even on high-resolution imaging, the edges of the SE image have worse contrast than the rest of the image, hence ellipse fitting works with higher error at these regions. Another crucial factor is that more than one intensity maximum can belong to an individual prism, especially when the long axis of the prism lies in the plane of the image (perpendicular to the incident electron beam). In this case, the number of prisms and the average inclination angle increase.

Adjustment of the appropriate threshold for the intensities is a key factor of pre-processing. Ellipse fitting after a well-adjusted threshold and a typically wrong selected one can be see in Figure 2. The difference between the threshold of the two images is 23%. The average azimuthal angle remained the same, however the number of ellipses increased from 46 to 57 (real prism number: 45) due to the changing number of intensity maxima. Due to the more sensitive maximum finding process, individual prisms are displayed as separated ellipses (e.g., Figure 2c bottom left corner). However, despite the inappropriate threshold value, the majority of the prisms and their azimuthal angle were correctly found.

The accuracy of azimuthal and inclination angle of prisms was approximated by fitting ellipses on two areas with homogeneous but fundamentally different prism arrangements. For simplicity, intensity maxima, which belong to incomplete prisms, at the margin of the image were excluded from the representation and calculation on Figure 3a.

According to Figure 3c, the azimuthal angle falls in the narrow range of ∼53–60° when the elongation direction of prism is parallel to the cut surface of the cross-section (blue dots). This indicates better accuracy than in the perpendicular direction (green squares) and the accuracy increases with increasing aspect ratio. According to the visual observation of the SEM image (Figure 3a), the area is not perfectly homogeneous and therefore this scatter of azimuthal angle values should not be treated as the error. When prisms are perpendicular to the cross-sectional surface (Figure 3b), the distribution of the azimuthal angle practically covers the whole range, as the aspect ratio is low and small error in finding ellipse axes results larger deviation in azimuthal angles.

4 | RESULTS AND DISCUSSION

4.1 | Application 1. Prism arrangement parallel to the DEJ: Quantitative analysis of HSBs

A secondary-electron SEM image of the whole section of enamel shows several HSBs following the curvature of the DEJ (Figure 4a). Application of the ellipse fitting method and the resulting orientation map highlight the characteristics of prism arrangement through the entire thickness of the enamel and opens way for the application of statistical tools and performing quantitative analysis.

Ellipse fitting has been applied over the entire thickness of the studied enamel cross section (Figure 4). The resulting color coded orientation map provides a striking visualization of locally changing prism arrangement. Based on qualitative observation two features can be highlighted. First, identification of HSBs is more straightforward than on the raw SE image. Second, overall increase of reddish contribution from the bottom left towards the top right corner. This latter indicates a gradual shift of azimuthal angle towards 90°. As DEJ can be considered as a rotating coordinate system, the cca. 45° azimuthal angle

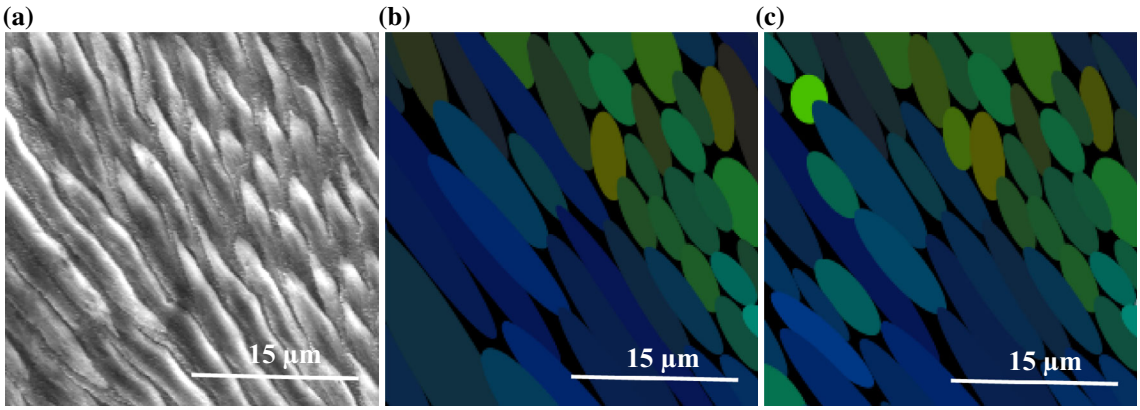

FIGURE 2 Sensitivity value of thresholding on a selected SEM region. Raw image (a), sensitivity value was set to 90 (46 ellipses found) (b), and to 70 (57 ellipses found) (c). Due to the higher sensitivity, more ellipse were fitted to the same amount of enamel prism.

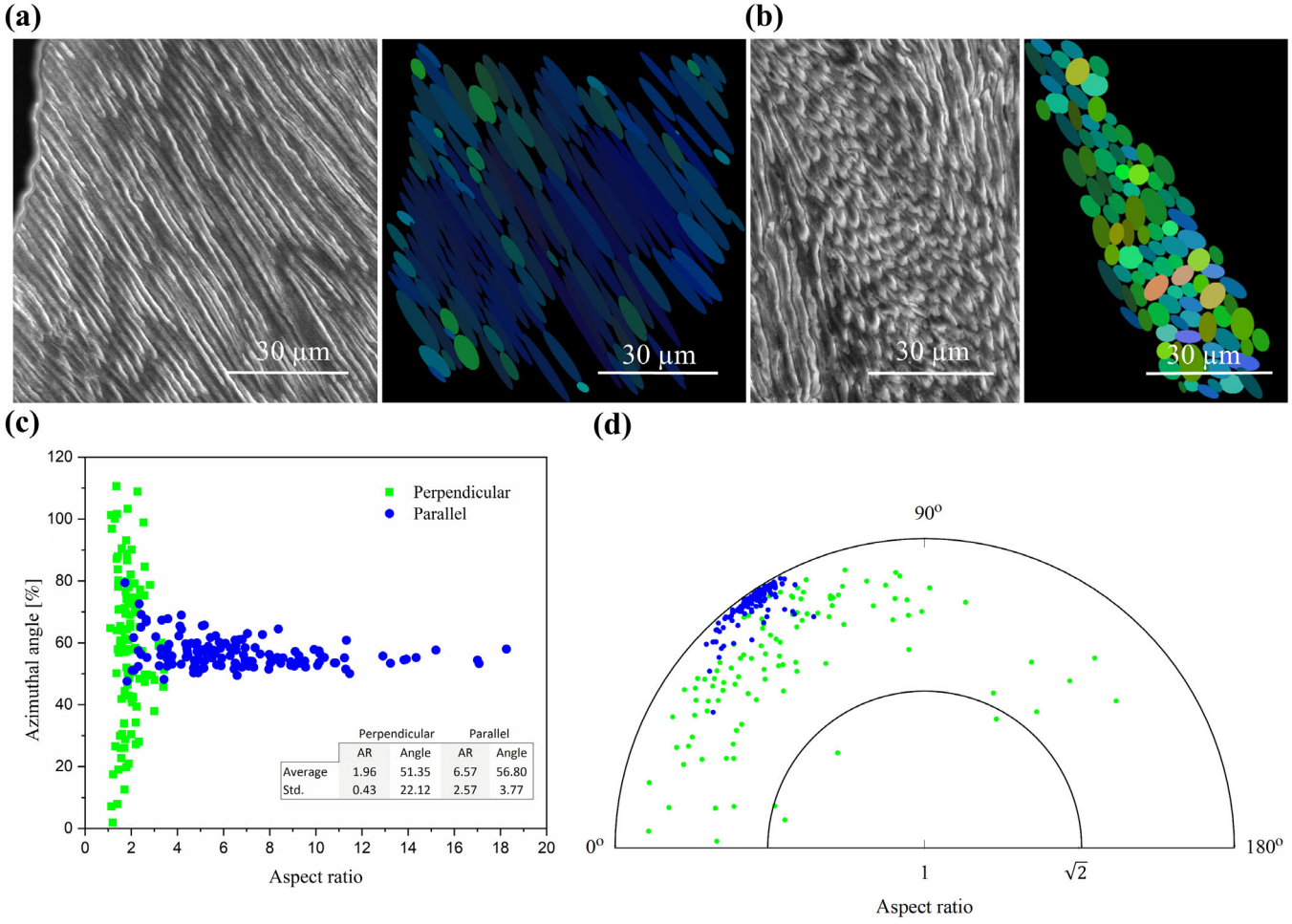

FIGURE 3 Accuracy of the ellipse fitting method illustrated on two areas with homogeneous prism arrangement. Elongation direction of prisms is nearly parallel to the cut surface close to the surface of the enamel (a), while prisms have ~60° inclination angle in a HSBs (b). Comparison of the accuracy of fitted ellipse parameters based on the two areas was done by plotting the distribution of azimuthal angle as function of aspect ratio (c and d). Colors represents the two analyzed areas for better separation and it is not comparable with the color code used before, blue: area (a) with prisms nearly parallel to the cut surface, green: area (b) with prisms perpendicular to the cut surface.

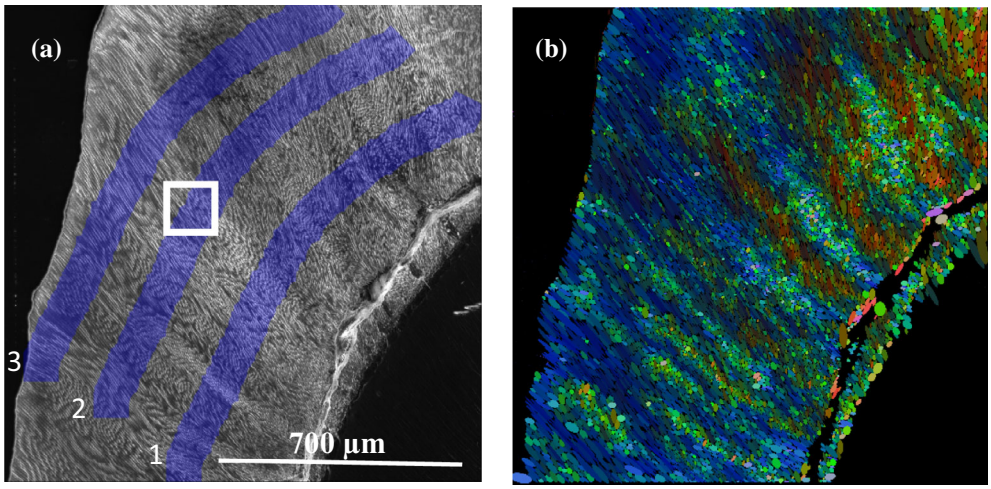

FIGURE 4 Secondary electron SEM image of enamel cross section. The continuous white line at the right hand side of Figure 4a marks a massive crack along the DEJ. Blue bands are selected for quantitative prism orientation analysis, presented in Figure 6. The white rectangle shows the area presented in Figure 1a (a). Prism orientation map of the same image. The colors represent the azimuthal angle and the aspect ratio of ellipses, according to Figure 1d (b).

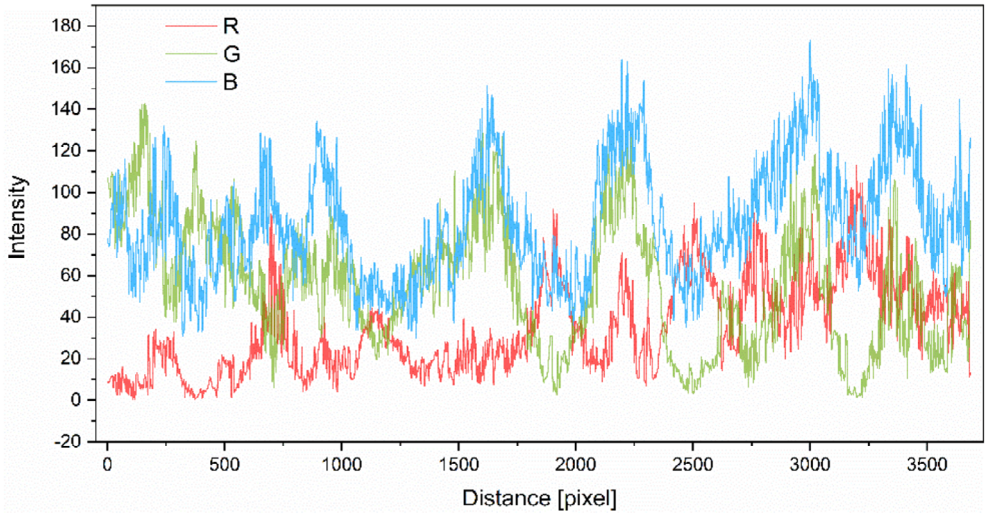

FIGURE 5 Raw RGB intensity profiles of band 1 on Figure 4b starting from the bottom left corner. Red and blue values represent azimuthal angle and green shows the change of aspect ratio along the profile, as defined in Figure 1d.

difference between prisms along the DEJ indicate that to maintain the same anatomical position with respect to DEJ prisms follow its curvature.

To perform quantitative analysis of prism orientation through the HSBs, approximately 100 µm wide bands were selected parallel, but at different distance to the DEJ (blue shade in Figure 4a). Band 1 is located near the DEJ, band 2 is at the end of HSBs, and band 3 is in the outer area of the enamel. Along the length of the selected bands prism arrangement was analyzed by averaging numerical data extracted from the orientation maps (i.e., color information) in the width of the bands at a given distance in pixels from the arbitrary chosen starting point (bottom left corner). The averaged RGB components are shown in Figure 5 for band 1. All RGB components exhibit strong variation as function of position, following the periodicity of prism orientation across the HSBs. The borders of the HSBs are marked by the minima along the curve of the green component, which indicates the smallest aspect ratio, i.e. prism cross section closest to circle. Increasing average intensity of red component indicates gradual rotation of azimuthal angles with the curvature of the DEJ.

In order to quantify the average orientation variation, azimuthal and inclination (vertical) angles were calculated back from the RGB values of the orientation map (Figure 4b) using Equations (1)–(3), and plotted in Figure 6 as function of position for all three bands. All three line profiles of azimuthal angle exhibit the rotation of enamel prisms, following the curvature of DEJ, which now can be quantitatively assessed. As the length in micrometer of bands 1, 2, and 3 is the same, band 1 close to the DEJ exhibits the largest increase of azimuthal angle (from 57.5° to 79.4°), while the change of azimuthal angle along band 3 is the lowest (from 84.2° to 89.7°).

To improve statistics, smoothing by adjacent-averaging of 20 points was applied. Such xy-type plots allow to define numerically the border and width of HSBs based on the same criteria through the whole cross section. In the present case, AR = 2.5 was set as the upper limit for a HSB, which corresponds to 66.5° inclination angle. Note that this value is an averaged value calculated from the 100 µm wide band and subsequently smoothened by adjacent averaging of 20 data points. By changing these parameters, different numerical results can be obtained, which calls the attention to the role of

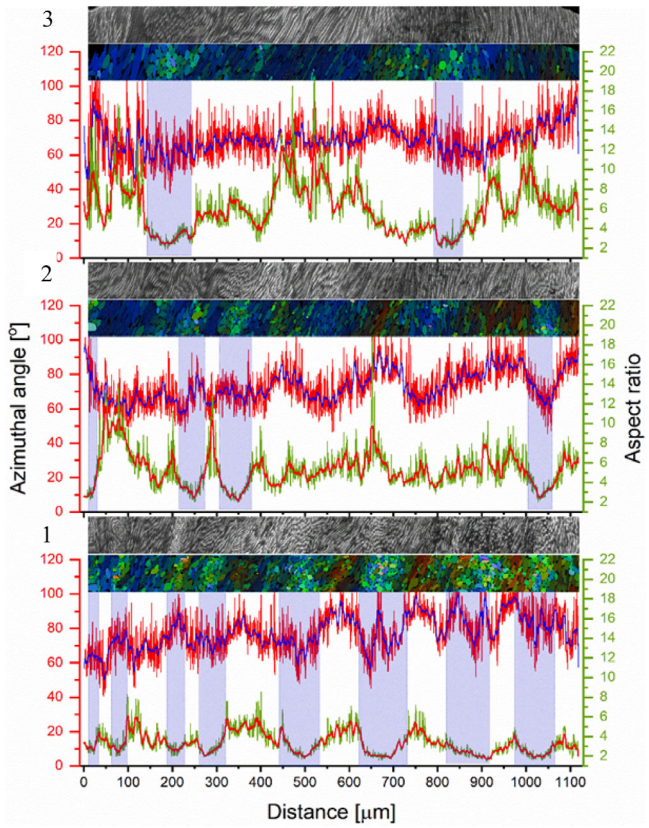

FIGURE 6 Aspect ratio and azimuthal angle line profiles obtained from RGB values of the orientation maps along the bands 1, 2, and 3 marked on Figure 4a. Selected areas on SEM and color coded ellipse fitted images corresponding to the bands were straightened for easier comparison. Low aspect ratio segments (AR <2.5) of the profiles are highlighted by transparent blue, which correspond to HSBs. Blue and red lines show the smoothened raw profiles by applying 20 points adjacent-averaging.

using a proper statistical setup consequently. Based on the applied criteria eight HSBs were identified in band 1, while in bands 2 and 3 the number of HSBs lower, four and two, respectively. The width of the HSBs varies between 37.2–111.5, 57.5–78.5 and 74.4–99.1 along the bands 1, 2, and 3, respectively.

4.2 | Application 2. Small scale variation of prism arrangement from the enamel external surface to the DEJ

Prism arrangement varies at smaller scale as well. Based on the orientation map (Figure 4b), the azimuthal angle of prisms located inside (AR <2.5) and outside (AR≥2.5) of the HSBs is systematically different. In order to quantify this difference, two parallel, adjacent areas were selected starting from the enamel external surface (Figure 7a). Close to the enamel external surface (outermost 300 μm) no statistically meaningful difference of azimuthal angles can be detected between the two areas. However in the middle part (approximately 300–500 μm from the outer surface) the azimuthal angle in the two adjacent areas varies as function of prism arrangement of the inner parts (from 500 μm to DEJ). If there is a HSB, that is, prisms are rotated out of the plane of the section, azimuthal angle of prisms in the middle part (300–500 μm) decreases down to a minimum value of 36°. Between the HSBs, where the prisms lay approximately in the plane of the section, azimuthal angle of prisms in the middle part (300–500 μm) remains uniformly around 63° (Figure 7b). In the innermost part (from 500 μm to DEJ), which is practically the zone of the HSBs, the average azimuthal angle in- and outside of the HSB coincides. By inspecting azimuthal angle line profiles on Figure 7b, the separation of the in-HSB and out-of-HSB curves in the 300–500 μm zone is clearly seen. This tendency of azimuthal angle along the thickness of the enamel is apparently opposite to the variation of inclination angle (Figure 7c). We note that due to the large azimuthal angle error inside HSBs related to the small aspect ratio of ellipses, the angle variation inside the band has not been analyzed.

These small scale systematic variations of azimuthal angles can be easily observed and quantified using *xy*-plots constructed based on orientation maps, while they remain hidden during visual assessment of SEM images or when using light microscopy (Lynch et al., 2010).

4.3 | Perspectives of the presented quantitative image analysis method

Prisms are fundamental microscale building units of mammalian dental enamel, which formation is controlled by the activity of ameloblasts (Lester & von Koenigswald, 1989; Osborn, 1965). From the point of view of the nanostructure, the prisms can be considered as a quasi-periodic framework for the gradually changing crystallographic orientation of HAP nanocrystals, as indicated by nanocrystal orientation mapping on the hundreds of prisms scale (Beniash et al., 2019).

While nanocrystal orientation mapping of whole cross sections of dental enamel relies on several well established and state-of-the-art techniques like synchrotron X-ray diffraction (Al-Jawad et al., 2007; Free et al., 2022; Raue et al., 2012; Simmons et al., 2011) (for a recent review, see Besnard et al. (2023)) or transmission electron back scattered diffraction (Koblischka-Veneva et al., 2018), the analysis of prism orientation mainly comprise qualitative evaluation of light microscopy or SEM images, there are only a few quantitative data regarding the prism pattern observed using these methods (e.g., Lynch et al., 2010; Rensberger, 1997). Enamel prisms, according to the movement of ameloblasts during amelogenesis, follow a wavy pathway from the DEJ to the enamel external surface (Osborn, 1965). Thus, when enamel microstructure is investigated over an entire tooth cross section using imaging methods, a single prism never can be traced along its whole length. The image then shows a two-dimensional pattern, according to the locally changing shape of prism cross sections. Three dimensional arrangement can be either reconstructed based on series of 2D patterns or investigated using tomographic methods.

A recent report presents a unique three-dimensional investigation of prism arrangement using X-ray tomography combined with

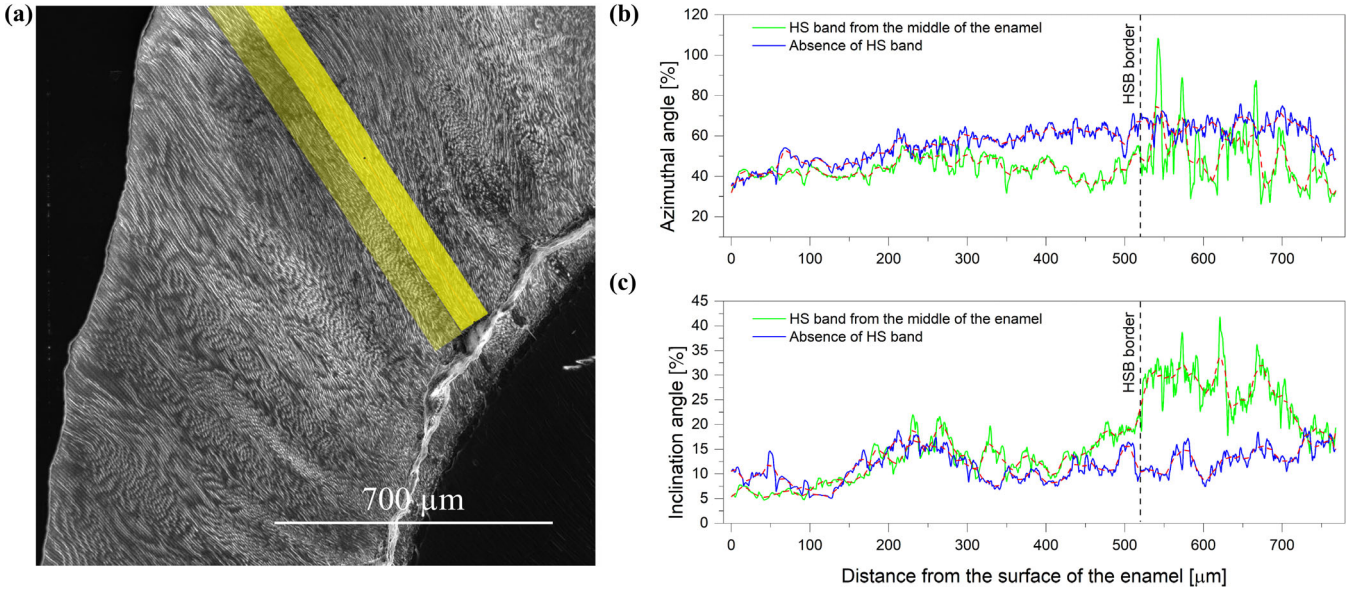

FIGURE 7 Selected areas for line profile analysis starting from the external enamel surface and ending in a HSB (pale yellow) and next to the band (bright yellow) (a). Azimuthal (b) and inclination angle line profiles (c) of areas of Figure 4a. For better visibility, smoothing by adjacent-averaging of 20 points was applied. Note that based on the large azimuthal angle error inside HSBs due to the small aspect ratio of ellipses, the angle variation inside the band has not been analyzed.

slice-and-view FIB-SEM study (Besnard, Marie, Buček, et al., 2022), which allows the reconstruction of fine details of prism structure in three dimensions. X-ray tomography is able to reveal large volumes at the required resolution, however, requires extensive computation capacity during the 3D reconstruction. Accordingly, only a subvolume (approx. 200 × 200 × 130 µm) of enamel was subjected to the analysis in (Besnard, Marie, Buček, et al., 2022). On the other hand, FIB-SEM is a local method, and thus, between the analyzed approximately 5 µm sized electron transparent lamellae, interpolation is required. We believe that the application of the presented image processing method on successively obtained images can be a reasonable alternative of the slice-and-view FIB for the analysis of 3D prism orientation over entire enamel cross section. At the same time, we highlight that our method performed on a single image does not provide a full 3D reconstruction of prism arrangement, but has the advantage of being local in terms of thickness on the micrometer scale. Thus, allows to correlate mechanical, compositional or structural data from the uppermost few micrometer thick layer with prism orientation in an anatomically defined cross section.

The proposed simple method can be performed on SEM images obtained using easily accessible laboratory microscopes. Thanks to the numerical parameters rendered to each prism cross section, variation of prism orientation in the imaged plane can be interpreted visually and analyzed quantitatively. Color coded maps and line profiles allow further quantification of the variation of prism arrangement along the image plane. The investigation of HSBs can be performed using statistical tools, which reduce the subjectivity and enhance reproducibility of the analyses. Quantitative comparison allows an improved interpretation of regional variations in HSB distribution (Lynch et al., 2010). Also, it may provide useful insight into ameloblast activity during enamel formation (Hanaizumi et al., 2010) and boost evolutionary aspects of enamel investigation as well (Sahni, 1987b).

Enamel prism orientation is a mesoscale approximation of average nanocrystal orientation (Beniash et al., 2019; Free et al., 2022). Quantification of prism arrangement and fine details of prism orientation distribution and HSB patterns (e.g., Figure 7b) allow a deeper understanding of the relation between nanocrystal orientation distribution and mechanical performance. The developed method has been used for the quantitative assessment of prism arrangement in human tooth enamel in order to determine the prism orientation dependency of mechanical parameters (Hegedűs et al., 2023). Moreover, quantitative comparisons between enamel microstructures and enamel tissue engineering products may promote enamel biomimetics and material design (Pandya & Diekwisch, 2019).

5 | CONCLUSIONS

The presented image processing method allows a quantitative assessment of the microstructure of enamel at prism size resolution. The SE images of etched cross sectional surfaces are processed and each prism cross section is approximated with ellipses. Geometrical parameters of the ellipses (aspect ratio and major axis direction) are used to quantify prism orientation in terms of azimuthal and inclination angles, with respect to the imaged cross section. Orientation maps are constructed by assigning color codes to these angle parameters, in the ranges and 0°–180° and 0°–90°, respectively. Limitations and accuracy of the image processing method were analyzed. The application of the image processing method was demonstrated for the analysis of HSBs in a bucco-lingual section of a sound molar. Orientation

parameters were retrieved from color coded orientation maps and the number, boundaries, and width of HSBs as function of distance from the DEJ were determined and compared quantitatively. The presented ellipse fitting method allows an automatic quantitative evaluation and statistical analysis of thousands of enamel prisms and provides a simple, *xy* plot-like description of the variation of characteristic prism parameters within the same image. Moreover, assigning the image with color codes based on the azimuthal angle and aspect ratio of prims, makes HSBs more easily visible and reveals the fine details and orientation changes.

We believe that the introduced image processing method can be applied in several fields of dental research and restorative treatments. The vivid color coded image can help to find the desirable area for mechanical studies where the orientation of the enamel prisms can be an important factor. The method can be used in evolutionary biology, for the analysis of HSBs, which can provide deeper insight into the evolution of the enamel formation and correlation with dietary habits. Quantitative comparison of enamel prism patterns of different species may facilitate to understand how the enamel formation process has evolved over time and reveal the details of the evolutional changes of ameloblast and amelogenin by observing the end product of their operation.

AUTHOR CONTRIBUTIONS

Máté Hegedűs: Investigation; methodology; visualization; writing – original draft; data curation. **Viktória Kovács Kis:** Supervision; writing – review and editing; funding acquisition. **Zsolt Kovács:** Supervision; methodology; visualization; writing – review and editing. **Noémi Rózsa:** Writing – review and editing.

ACKNOWLEDGMENTS

This work was supported by the National Research, Development and Innovation Fund Office, Hungary, under the Project "Investigation of the nanostructural background of functionality in case of biogenic and biocompatible mineral apatite", grant number K-125100.

DATA AVAILABILITY STATEMENT

Data will be made available on request.

ORCID

Máté Hegedűs https://orcid.org/0000-0002-8003-212X

REFERENCES

Al-Jawad, M., Steuwer, A., Kilcoyne, S. H., Shore, R. C., Cywinski, R., & Wood, D. J. (2007). 2D mapping of texture and lattice parameters of dental enamel. *Biomaterials*, *28*(18), 2908–2914. https://doi.org/10.1016/j.biomaterials.2007.02.019

An, B., Wang, R., & Zhang, D. (2012). Role of crystal arrangement on the mechanical performance of enamel. *Acta Biomaterialia*, *8*(10), 3784–3793. https://doi.org/10.1016/j.actbio.2012.06.026

Arnold, W. H., Haddad, B., Schaper, K., Hagemann, K., Lippold, C., & Danesh, Gh. (2015). Enamel surface alterations after repeated conditioning with HCl. *Head & Face Medicine*, *11*(1). https://doi.org/10.1186/s13005-015-0089-2

Bajaj, D., & Arola, D. (2009). Role of prism decussation on fatigue crack growth and fracture of human enamel. *Acta Biomaterialia*, *5*(8), 3045–3056. https://doi.org/10.1016/j.actbio.2009.04.013

Beniash, E., Stifler, C. A., Sun, C.-Y., Jung, G. S., Qin, Z., Buehler, M. J., & Gilbert, P. U. P. A. (2019). The hidden structure of human enamel. *Nature Communications*, *10*, 4383. https://doi.org/10.1038/s41467-019-12185-7

Besnard, C., Marie, A., Buček, P., Sasidharan, S., Harper, R. A., Marathe, S., Wanelik, K., Landini, G., Shelton, R. M., & Korsunky, A. M. (2022). Hierarchical 2D to 3D micro/nano-histology of human dental caries lesions using light. *X-Ray and Electron Microscopy, Materials & Design*, *220*, 110829. https://doi.org/10.1016/j.matdes.2022.110829

Besnard, C., Marie, A., Sasidharan, S., Harper, R. A., Shelton, R. M., Landini, G., Korsunsky, A. M. (2023) Synchrotron X-ray studies of the structural and functional hierarchies in mineralised human dental enamel: A state-of-the-art review, *Dental Journal*; *11*(4):98. https://doi.org/10.3390/dj11040098.

Chu, K., Zhao, C., & Ren, F. (2021). Measuring fracture toughness of human dental enamel at small scale using notched microcantilever beams. *Biosurface and Biotribology*, *7*(4), 228–232. https://doi.org/10.1049/bsb2.12022

Cui, F. Z., & Ge, J. (2007). New observations of the hierarchical structure of human enamel, from nanoscale to microscale. *Journal of Tissue Engineering and Regenerative Medicine*, *1*(3), 185–191. https://doi.org/10.1002/term.21

Daculsi, G., & Kerebel, B. (1978). High-resolution electron microscope study of human enamel crystallites: Size, shape, and growth. *Journal of Ultrastructure Research*, *65*, 163–172. https://doi.org/10.1016/S0022-5320(78)90053-9

Daculsi, G., Menanteau, J., Kerebel, L. M., & Mitre, D. (1984). Length and shape of enamel crystals. *Calcified Tissue International*, *36*(1), 550–555. https://doi.org/10.1007/BF02405364

Evans, A. R., Wilson, G. P., Fortelius, M., & Jernvall, J. (2006). High-level similarity of dentitions in carnivorans and rodents. *Nature*, *445*(7123), 78–81. https://doi.org/10.1038/nature05433

Ferrario, V. F., Sforza, C., & Zanotti, G. (2004). Maximal bite forces in healthy young adults as predicted by surface electromyography. *Journal of Dentistry*, *32*, 451–457. https://doi.org/10.1016/j.jdent.2004.02.009

Free, R., DeRocher, K., Cooley, V., Xu, R., Stock, S. R., & Joester, D. (2022). Mesoscale structural gradients in human tooth enamel. *Proceedings of the National Academy of Sciences of the United States of America*, *119*(52), e2211285119. https://doi.org/10.1073/pnas.2211285119

Hanaizumi, Y., Yokota, R., Domon, T., Wakita, M., & Kozawa, Y. (2010). The initial process of enamel prism arrangement and its relation to the Hunter-Schreger bands in dog teeth. *Archives of Histology and Cytology*, *73*(1), 23–36. https://doi.org/10.1679/aohc.73.23 PMID: 21471664.

He, L.-H., Yin, Z.-H., van Vuuren, L. J., Carter, E. A., & Liang, X.-W. (2013). A natural functionally graded biocomposite coating—Human enamel. *Acta Biomaterialia*, *9*(5), 6330–6337. https://doi.org/10.1016/j.actbio.2012.12.029

Hegedűs, M., Kis K, V., Szabó, Á., Kovács, I., Rózsa, N., & Kovács, Z. (2023). Gradient structural anisotropy of dental enamel is optimized for enhanced mechanical behaviour. *Materials & Design*, *234*, 112369. https://doi.org/10.1016/j.matdes.2023.112369

Hogg, R. T., & Elokda, A. (2021). Quantification of enamel decussation in gracile and robust capuchins (Cebus, Sapajus, Cebidae, Platyrrhini). *American Journal of Primatology*, *83*(5), e23246. https://doi.org/10.1002/ajp.23246

Hogg, R. T., & Richardson, C. (2019). Application of image compression ratio analysis as method for quantifying complexity of dental enamel microstructure. *The Anatomical Record*, *302*(12), 2279–2286. https://doi.org/10.1002/ar.24261

Ishiyama, M. (1984) Comparative histology of tooth enamel in several toothed whales. In: *Tooth enamel IV*, Elsevier BV Fearnhead RW, Suga S (Eds): 432-436.

Koblischka-Veneva, A., Koblischka, M. R., Schmauch, J., & Hannig, M. (2018). Human dental enamel: A natural nanotechnology masterpiece investigated by TEM and t-EBSD. *Nano Research*, *11*, 3911–3921. https://doi.org/10.1007/s12274-018-1968-1

Lester, K. S., & von Koenigswald, W. (1989). Crystallite orientation discontinuities and the evolution of mammalian enamel or, when is a prism? *Scanning Microscopy*, *3*, 645–663.

Lucas, P., Constantino, P., Wood, B., & Lawn, B. (2008). Dental enamel as a dietary indicator in mammals. *BioEssays*, *30*(4), 374–385. https://doi.org/10.1002/bies.20729

Lynch, C. D., O'Sullivan, V. R., Dockery, P., McGillycuddy, C. T., & Sloan, A. J. (2010). Hunter-Schreger Band patterns in human tooth enamel. *Journal of Anatomy*, *217*, 106–115. https://doi.org/10.1111/j.1469-7580.2010.01255.x

Nanci, A. (2017). *Ten Cate's Oral histology* (9th ed.). Elsevier ISBN: 9780323485180.

Osborn, J. W. (1965). The nature of the Hunter-Schreger bands in enamel. *Archives of Oral Biology*, *10*, 929–935. https://doi.org/10.1016/0003-9969(65)90086-5

Pandya, M., & Diekwisch, T. G. H. (2019). Enamel biomimetics-fiction or future of dentistry. *International Journal of Oral Science*, *11*(1), 8. https://doi.org/10.1038/s41368-018-0038-6

Radlanski, R. J., Renz, H., Willersinn, U., Cordis, C. A., & Duschner, H. (2001). Outline and arrangement of enamel rods in human deciduous and permanent enamel. 3D-reconstructions obtained from CLSM and SEM images based on serial ground sections. *European Journal of Oral Sciences*, *109*(6), 409–414. https://doi.org/10.1034/j.1600-0722.2001.00149.x

Raue, L., Gersdorff, N., Rödiger, M., & Klein, H. (2012). New insights in prism orientation within human enamel. *Archives of Oral Biology*, *57*(3), 271–276. https://doi.org/10.1016/j.archoralbio.2011.08.015

Rensberger, J. M. (1997). Mechanical adaptation in enamel. In W. von Koenigswald & P. M. Sander (Eds.), *Tooth enamel microstructure* (pp. 237–257). A.A. Balkema.

Rensberger, J. M., & von, Koenigswald, W. (1980). Koenigswald, functional and phylogenetic interpretation of enamel microstructure in rhinoceroses. *Paleobiology*, *6*(4), 477–495.

A. Sahni (1987) Evolutionary aspects of reptilian and mammalian enamel structure, *Scanning Microscopy*, *1*(4), 1903–1912, Article 38.

Salvati, E., Besnard, C., Harper, R. A., Moxham, T., Shelton, R., Landini, G., & Korsunsky, A. M. (2019). Crack tip stress field analysis of crack surface contact and opening during in situ wedge loading of human enamel. *Key Engineering Materials*, *827*, 85–91. https://doi.org/10.4028/www.scientific.net/KEM.827.85

Simmons, L. M., Al-Jawad, M., Kilcoyne, S. H., & Woods, D. J. (2011). Distribution of enamel crystallite orientation through an entire tooth crown studied using synchrotron X-ray diffraction. *European Journal of Oral Sciences*, *119*, 19–24. https://doi.org/10.1111/j.1600-0722.2011.00909.x

Smith, C. E., Y, Hu, C.-C., Hu, J., & Simmer, J. P. (2019). Characteristics of the transverse 2D uniserial arrangement of rows of decussating enamel rods in the inner enamel layer of mouse mandibular incisors. *Journal of Anatomy*, *235*, 912–930. https://doi.org/10.1111/joa.13053

Smith, T. M., Olejniczak, A. J., Zermeno, J. P., Tafforeau, P., Skinner, M. M., Hoffmann, A., & Hublin, J.-J. (2012). Variation in enamel thickness within the genus homo. *Journal of Human Evolution*, *62*(3), 395–411. https://doi.org/10.1016/j.jhevol.2011.12.004

Tafforeau, P., Zermeno, J. P., & Smith, T. M. (2012). Tracking cellular-level enamel growth and structure in 4D with synchrotron imaging. *Journal of Human Evolution*, *62*(3), 424–428. https://doi.org/10.1016/j.jhevol.2012.01.001

Wilmers, J., & Bargmann, S. (2020). Nature's design solutions in dental enamel: Uniting high strength and extreme damage resistance. *Acta Biomaterialia*, *107*, 1–24. https://doi.org/10.1016/j.actbio.2020.02.019

Yang, D., Bharatiya, M., Grine, F. E., & Band, H.-S. (2022). Configuration in human molars reveals more decussation in the lateral enamel of 'functional' cusps than 'guiding' cusps. *Archives of Oral Biology*, *142*, 105524, ISSN 0003-9969. https://doi.org/10.1016/j.archoralbio.2022.105524

How to cite this article: Hegedűs, M., Kis, V. K., Rózsa, N., & Kovács, Z. (2023). A novel image processing procedure for the quantitative evaluation of dental enamel prism arrangement. *Microscopy Research and Technique*, 1–10. https://doi.org/10.1002/jemt.24473